Made available by Hasselt University Library in https://documentserver.uhasselt.be

Assessing the in vivo toxicity of titanium dioxide nanoparticles in Schmidtea mediterranea: uptake pathways and (neuro)developmental outcomes

Peer-reviewed author version

LEYNEN, Nathalie; TYTGAT, Julie; BIJNENS, Karolien; JAENEN, Vincent; Verleysen, Eveline; ARTOIS, Tom; VAN BELLEGHEM, Frank; SAENEN, Nelly & SMEETS, Karen (2024) Assessing the in vivo toxicity of titanium dioxide nanoparticles in Schmidtea mediterranea: uptake pathways and (neuro)developmental outcomes. In: AQUATIC TOXICOLOGY, 270 (Art N° 106895).

DOI: 10.1016/j.aquatox.2024.106895
Handle: http://hdl.handle.net/1942/42972

Assessing the *in vivo* toxicity of titanium dioxide nanoparticles in *Schmidtea mediterranea*: uptake pathways and (neuro)developmental outcomes

Leynen N.*[1], Tytgat JS.*[1], Bijnens K.[1], Jaenen V.[1], Verleysen. E.[3] ;Artois T.[1], Van Belleghem F.[1,2], Saenen ND.[1], Smeets K.[1]

*** co-first authorship**

Corresponding author: karen.smeets@uhasselt.be (K. Smeets)

1. Centre for Environmental Sciences, Zoology, Biodiversity and Toxicology; Hasselt University; Hasselt; Belgium.
2. Department of Environmental Sciences; Faculty of Science; Open Universiteit; Heerlen; the Netherlands.
3. Trace Elements and Nanomaterials, Sciensano, Groeselenbergstraat 99, 1180 Uccle, Belgium

Abstract

Titanium dioxide nanoparticles (TiO_2-NPs) are present in the aquatic environment as a result of urban run-off, product use and post-consumer degradation, and interact with aquatic organisms through water and sediments. To conduct a thorough toxicity assessment, it is crucial to have comprehensive data covering all compartments of the aquatic ecosystem. Currently, however, there is a notable lack of such data, especially concerning the benthic zone. In the current work, we used the planarian *Schmidtea mediterranea* to investigate the effects of TiO_2-NPs (5 mg/L and 50 mg/L). Planarians are benthic organisms that play an important role in the food chain as predators. Our study integrated toxicokinetic and toxicodynamic parameters and showed that the uptake of TiO_2-NPs of 21 nm occurred through the epidermis and intestine. Epidermal irritation and mucus production were immediately present after exposure. Furthermore, we observed that TiO_2-NPs induced stronger effects in regenerating organisms. TiO_2-NPs interfered with neuroregeneration, inducing behavioral effects. A delay in the formation of the anterior commissure between the two brain lobes after seven and nine days of

exposure to 50 mg/L was observed, probably as a result of a decreased stem cell proliferation. Based on our data, we advocate for the incorporation of multiple exposure routes into toxicity screenings. Additionally, we emphasize the vulnerability of developing organisms and recommend their inclusion in future risk assessment strategies.

Keywords

Titanium dioxide; Nanoparticles; Planarians; Regeneration; Neurodevelopment; Uptake; Toxicity

Graphical abstract

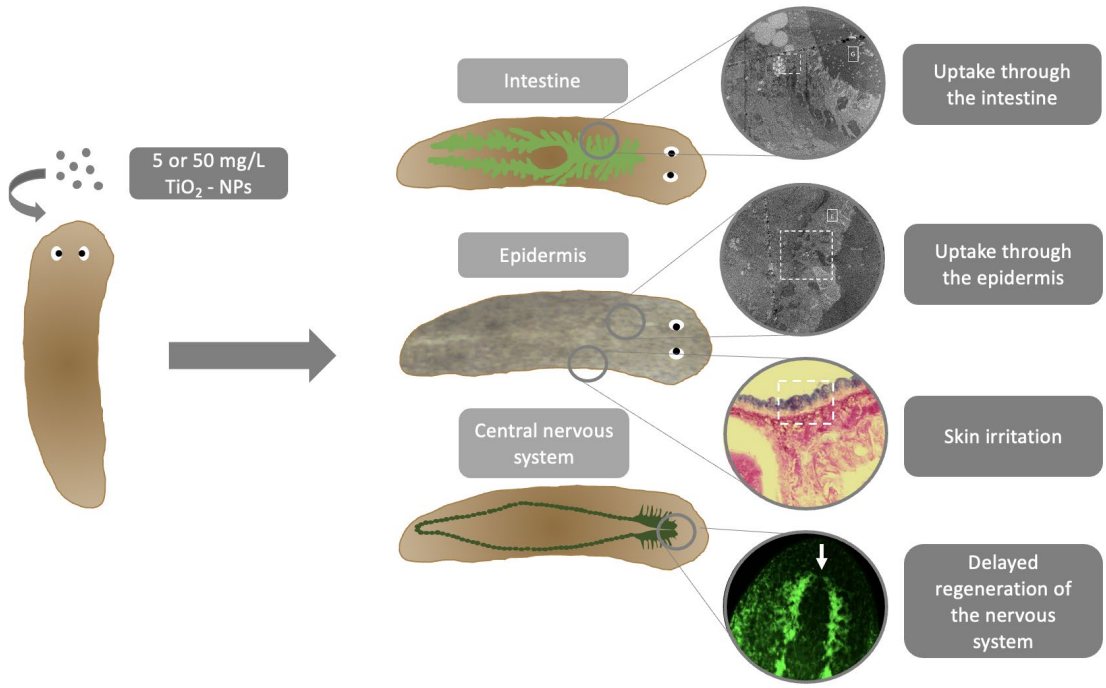

1. Introduction

Titanium dioxide (TiO_2) is a widely produced nanoparticle that serves as a pigment or a photocatalyst and is used in a wide range of products such as; white paint, toothpaste, sunscreen and cosmetic products (Boutillier et al. 2020). TiO_2 was recently banned by the European Commission (European Commission 2022) as a food additive (E171), as it was no longer considered safe by the European Food Safety Authority (EFSA) in 2021 (EFSA 2021). Nanoparticles are particles with one or more dimensions in the order of 100 nm or less (ISO 2021). Due to their size and surface area, nanomaterials may have unique chemical, physical, electrical, and mechanical properties that are more pronounced compared to the bulk material (Joudeh and Linke 2022). In addition, the same nanomaterial can occur in different shapes or can have different surface charges and modifications. All these properties will have an impact on the uptake and toxicity of the particle. For example, a smaller size and greater surface area will result in increased uptake and interaction with biological tissues (Abbasi et al. 2023), or a positively charged NP will be more effectively internalised because of the negative charge of the cell membrane, resulting as well in more toxic effects (Akanksha et al. 2019).

Nanoparticles can be present in the aqueous phase or can aggregate and precipitate due to their physicochemical properties, making it important to assess the effects of nanoparticles on different compartments of the ecosystem. In surface water, TiO_2-NPs are found at levels up to 0.021 mg/L, varying between places and times (Gottschalk et al. 2009). Parker and Keller (2019) measured peak concentrations of 1.490 mg/L TiO_2-NPs in a freshwater compartment in Los Angeles and a minimum concentration of 0.243 mg/L TiO_2-NPs in Des Moines, varying with meteorological conditions. Sediments, on the other hand, generally contain higher TiO_2-NP concentrations. In the ocean, sediment levels of TiO_2-NPs peaked at 123 mg/kg in 2020 (Zheng and Nowack 2021), while freshwater systems showed simulated concentrations up to 25 mg/kg (Jovanović et al. 2016). Animals living in the benthic zone of the aquatic body are thus expected to be at a higher risk for toxicological effects given their higher exposure concentrations and durations.

Only a few studies investigated the effects of TiO_2-NPs on benthic and epi-benthic organisms, e.g., planarians and crustaceans. In *Atya lanipes* (freshwater shrimp) TiO_2-NPs (1.0, 10.0, 50.0, 100.0, and 150.0 mg/L) caused an increase in mortality, hyperactivity, and morphological changes like less pigmentation and the presence of edema after 48 and 72 h exposures (Cruz-Rosa and Pérez-Reyes 2023). TiO_2-NPs (4 mg/L) significantly reduced energy assimilation after 30 days in the freshwater amphipod *Gammarus fossarum* (Luderwald et al. 2019). In addition, TiO_2-NPs had toxic effects on *Hydropsyche exocellata* after 14 days of exposure (50

mg/L) with an increased mortality, and effects on lipid peroxidation (increased) and catalase (decreased) (Torres-Garcia et al. 2020). Also, in other freshwater and marine organisms inhabiting the water column, toxicity effects varied based on the properties of the particles or the specific organism exposed. *Daphnia magna* showed delayed reproduction and an altered heart morphology after exposure to 37.5 - 600 mg/L of TiO_2-NPs (15.1 nm) (Mendoza-Villa et al. 2023). In zebrafish, TiO_2-NPs of 21 nm (0.01 - 1 mg/L) affected motor behavior and neurodevelopment, along with a hindered growth of the axonal neurons (Gu et al. 2021).

Our study aims to address the reported variation by integrating physicochemical characteristics with toxicokinetics and -dynamics, examining effects across different developmental stages. We used the planarian species *S. mediterranea* as a model organism. *S. mediterranea* is a recognised model for assessing chemical and particle developmental toxicity (Hagstrom et al. 2015, Leynen et al. 2019, Cesarini et al. 2023). *S. mediterranea* allows the restoration of lost and damaged cells and tissues in only seven days, including the nervous system (Scimone et al. 2014). This enables us to study development in detail and the effects of toxic compounds on these processes, along with the possibility of comparing damaging effects in adults and developing organisms. Moreover, planarians are promising bio-indicators for freshwater ecosystems as they undergo bioaccumulation, have sensitive functional and morphological endpoints, and play different roles (predator, prey) in the trophic aquatic system (Wu and Li 2018). Living in the benthic zone, planarians are exposed to elevated levels of nanoparticles, as sediments can form a sink for such pollutants, including titanium (Zheng and Nowack 2021). Overall, *S. mediterranea* serves as an excellent non-vertebrate model to assess developmental particle toxicity, in line with the 3 R (reduction, refinement, and replacement), NAM (new approach methods) principles, and REACH regulations (Hagstrom et al. 2015, Wu and Li 2018).

2. Materials and methods

2.1 TiO_2-NPs suspension and characterization

Spherical titanium dioxide nanoparticles (AEROXIDE P25, CAS 13463-67-7) with an external particle dimension of 21 nm were purchased from Degussa Evonik GmbH. This pure titanium dioxide powder (≥ 99.5% trace metals basis) consists of 80% anatase and 20% rutile TiO_2 and 'principal material' in toxicological research as a proxy for environmental TiO_2-NP exposure (OECD 2016). A stock suspension of 1 g/L TiO_2-NPs was prepared by dispersing the TiO_2-NP powder in ultrapure water with sonication (probe sonicator, MSE, amplitude 18). The stock

suspension was diluted with planarian cultivation medium to create an exposure medium of the desired concentration and then sonicated for 30 min to reduce agglomerates.

Transmission electron microscopy (TEM) samples were prepared using 1% Alcian blue treated positively charged carbon- and pioloroform coated 400 mesh copper grids (Agar Scientific, Stansted, Essex, UK). The grid was prepared using the grid-on-drop method by placing the grid on top of 20 µl of a 500 mg/L TiO_2-NPs stock suspension and incubating for 10 min, followed by a 1-min wash with ultrapure water to remove excess salts and contaminating material. The grids were dried from below with filter paper to avoid loss of the nanomaterial from the grid. TEM imaging was performed using a Philips EM 208 S operating at 60 kV, equipped with a charge-coupled device (CCD) TEM camera (Morada Soft Imaging System). Micrographs were taken randomly at 10 positions on the grid at a magnification of 56 kx.

The particles were characterized by quantitative TEM analysis. The dimensions of the constituent particles on the TEM images were analyzed via the ParticleSizer software, based on the standard operating procedure (SOP) 'Measurement of the minimal external dimension of the constituent particles of particulate materials from TEM images by the NanoDefine ParticleSizer software' (Nanodefine 2016) and the SOP description by Verleysen et al. (2019) as described in supplemental material and methods (Supplemental A.1).

Dynamic light scattering (DLS) measurements were performed with a Brookhaven Instruments Corporation DLS instrument. Intensity-based hydrodynamic diameter, zeta potential and dispersity index were measured from a 25 mg/L stock suspension and a 5 mg/L exposure medium immediately after diluting the TiO_2-NPs stock. In addition, DLS measurements were performed on the 25 mg/L exposure medium after the addition of the worms to examine the stability of the medium up to the third day. The DLS settings were 2.57 for the refractive index and 0.01 for the absorption parameter. The dispersant chosen was water (refractive index of 1.33).

2.2 Experimental design

2.2.1 Planarian cultivation

An asexual strain of the planarian *Schmidtea mediterranea* was cultivated in the dark with cultivation medium containing the following nutrients added to ultrapure water: 1.6 mM NaCl, 1.0 mM $CaCl_2$, 1.0 mM $MgSO_4$, 0.1 mM $MgCl_2$, 0.1 mM KCl and 1.2 mM $NaHCO_3$. The

cultivation medium had a pH of seven. The worms were kept in the dark at 20 °C and were fed veal liver once a week. At least seven days prior to an experiment, the animals were starved to avoid food-related influences on measured parameters. For all experiments, animals within a size range of 3 - 6 mm were used.

2.2.2 Planarian exposure and experimental setup

In this study, organisms were exposed to exposure media of 5 or 50 mg/L TiO_2-NPs. The concentrations used in this study were based on findings in the literature about environmental concentrations (Gottschalk et al. 2009, Jovanović et al. 2016, Parker and Keller 2019, Zheng and Nowack 2021) as well as on previous range-finding experiments by our research group. Additionally, in a previous study on AgNP toxicity, we observed effects on tissue- and neuroregeneration related to an altered stem cell cycle after exposure to 5 mg/L (Leynen et al. 2019). Similar concentration ranges for other NP types allow comparisons of particle dynamics and planarian responses in the future. The highest concentration used in our study (50 mg/L) allows comparison with other organisms, as concentrations of TiO_2-NPs within the range of 0.01 to 600 mg/L can be found in the literature with different organisms including *D. magna*, juvenile carp, crayfish and zebrafish (Gu et al. 2021, Mendoza-Villa et al. 2023). For the histological mucus measurements, an exposure concentration of 100 and 500 µg/L TiO_2-NPs was used. We used lower concentrations for these measurements since mucus production is seen as an initial defence mechanism (Oliveira et al. 2018). Within an experiment, the exposure medium was refreshed three times a week, to keep a stable exposure. Animals were always exposed in a six-well plate (9.07 cm^2/well) with five worms in each well and 5 ml of exposure solution per well. Figure 1 depicts an overview of the experimental timeline of this study. Experiments were performed on adult and regenerating worms. To induce regeneration, adult worms were cut transversely above the pharynx to obtain a head and a tail fragment. On day zero, the worms were exposed to TiO_2-NPs via the medium. Depending on the experiment, adult or regenerating animals were exposed for three, seven or fourteen days. At these specific time points, we studied behavior, mucus production, epidermal structure, regenerative success, neuronal aberrations and underlying stem cell dynamics. On day three, the mucus layer of adult worms was stained with Alcian blue/PAS and the presence of mucus in the culture medium was quantitatively and qualitatively measured using WGA. On day seven, the structure of the epidermal layer was visualized via hematoxylin and eosin (HE) staining. Brain ganglia in adult worms were visualized via immunohistochemistry (target: anti-synapsin) on day seven and day 14.

In heads and tail fragments, stem cell dynamics were studied using immunohistochemistry and fluorescence in situ hybridization (FISH) (targets: proliferating stem cells (H3P), general stem cell population (*Smedwi-1)* and differentiating stem cells (*NB21.11e*)) after three days and seven days of regeneration (abbreviated in the manuscript as dpa: days post-amputation). In addition, brain ganglia and axonal projections of sensory neurons were visualized via immunohistochemistry (targets: anti-synapsin and 1H6-E9, respectively) in seven-day (7 dpa) and 14-day (14 dpa) regenerating tail fragments. The cholinergic neurons (*ChAT*) were visualized after seven days of regeneration.

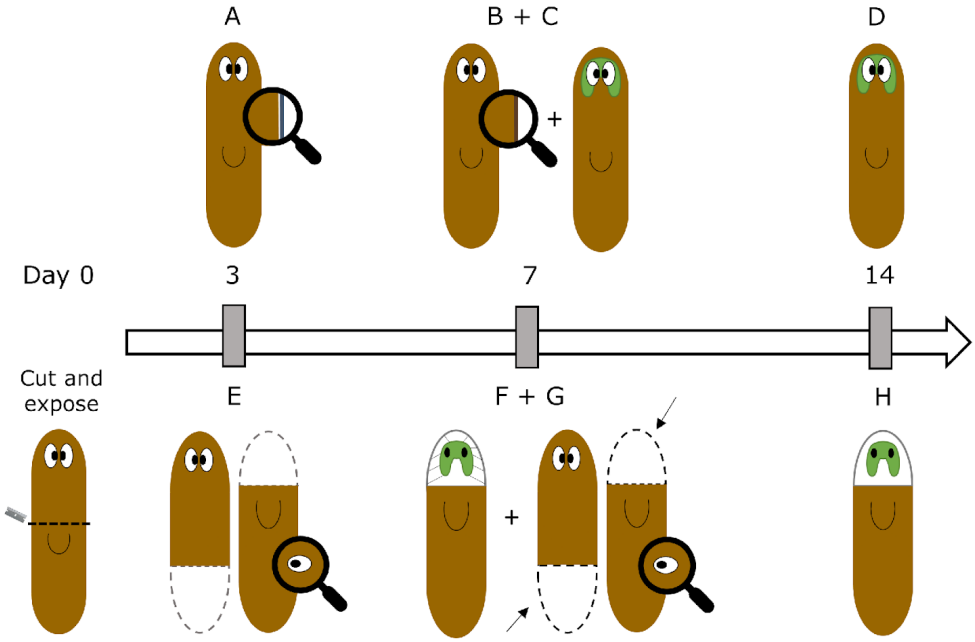

Figure 1: Timeline and experimental setup of this study. Experiments were performed on adult worms (above) and regenerating worms (below). Worms were exposed to TiO_2-NPs of 21 nm at day zero. For all experiments a concentration of 5 and 50 mg/L was used except for the mucus quantification via Alcian blue/PAS. Here a concentration of 100 and 500 µg/L was used. On day three, the mucus layer of adult worms was stained with Alcian blue/PAS to assess the thickness of the mucus layer (A). In addition, the mucus production was measured using WGA staining (A). On day seven, the epidermal layer (B) and brain ganglia degeneration (C) of adult worms was studied via HE stains and immunohistochemistry and FISH (targets: anti-synapsin*)*, respectively. On day 14, brain ganglia degeneration was visualized via immunohistochemistry via anti-synapsin (D). In three-day regenerating (3 dpa) head and tail fragments stem cell dynamics were studied via immunohistochemistry and FISH (targets: H3P,

Smedwi-1 and *NB21.11e*) (E). At 7 dpa, brain ganglia and axonal projections were stained in regenerating tails via immunohistochemistry and FISH (targets: anti-synapsin, 1H6-E9 and *ChAT*) (F), together with tissue regeneration (G) and stem cell dynamics in head and tail parts (H3P, *Smedwi-1* and *NB21.11e* via immunohistochemistry and FISH) (H).

2.3 Planarian behavior and general regeneration

Behavioral abnormalities were recorded in adults until eight days after exposure and regenerating fragments until 8 dpa, since planarians are able to regenerate their central nervous system in seven days and effects can be easily observed (Scimone et al. 2014). We focused on aberrant behavior, motility and negative phototaxis. In addition, the regenerating head and tail parts were subjected to two quantitative tests: the planarian locomotive velocity and the light avoidance behavior test to further quantify planarian behavior. More specifically, planarian velocity was assessed with a two-minute test as described by Lowe et al. (2015). Briefly, a Petri dish filled with cultivation medium was placed on a 0.5 cm grid. The planarian velocity was quantified as the number of lines the planarian head/tail crossed in two min, including 20 seconds of acclimatization after the addition of the worm to the Petri dish. Secondly, planarian negative phototaxis behavior was assessed using the light avoidance test (Inoue et al. 2004). Light avoidance was quantified as the time spent in the darkest region of a 60 x 25 mm box filled with cultivation medium. This box was divided into four regions and exposed to a cold light source, creating a gradient from high to low light intensity. Individual planarians were placed in the second-brightest region of the box. After 20 seconds of acclimatization, the time in the darkest region was recorded. Two experiments were performed, each with at least five individuals per condition.

To assess regenerative success, relative tissue regeneration was determined at 7 dpa by dividing the surface area of newly grown tissue (blastema) by the total body surface area. Digital images were acquired with a Nikon DS- Ri2 digital camera mounted on a Nikon SMZ800 stereomicroscope. Photographs were taken in triplicate per individual to minimize effects of movements on measurements, with a minimum of six worms per condition. Area measurements were performed in ImageJ (version 1.52n). This experiment was performed in triplicate. Planarian optic cups (hereinafter referred to as eyes) are composed of photoreceptors and pigment cells (Cebrià and Newmark 2007). As a marker of neurodevelopment, amputated tails (developing a head fragment) were scored for the presence of eye pigment cells (absent, faint or present) at 7 dpa to determine the success eye regeneration.

2.3 TiO_2-NPs localization in *Schmidtea mediterranea* tissues

2.3.1 Transmission electron microscopy (TEM)

Adult worms were injected with 100 nl of 1 g/L TiO_2-NPs stock suspension into the intestine, using Nanoject II (Drummond Scientific, Broomall, PA, USA). After three days of injection, the animals were fixed for TEM analysis. In addition, tails exposed to 50 mg/L TiO_2-NPs were fixed at 7 dpa. The fixation protocol is described in supplemental materials and methods (Supplemental A.2).

TEM observation and screening were performed using a Philips EM 208 S operating at 60 kV and equipped with a charge-coupled device (CCD) TEM camera (Morada Soft Imaging System). Digital micrographs were recorded and converted to TIFF format using TEM Imaging & Analysis software (Thermo Fisher Scientific).

2.3.2 HAADF-STEM-EDX

High-angle annular dark field scanning transmission electron microscopy (HAADF-STEM) and STEM-energy-dispersive X-ray spectrometry (STEM-EDX) were performed using a Talos F200S G2 scanning transmission electron microscope equipped with a HAADF detector and a Super-X EDS detector consisting of two windowless silicon drift detectors (Thermo Fisher Scientific). Tissue sections for HAADF-STEM-EDX were prepared in the same manner as described for TEM. STEM images were acquired at spot-size nine, with a scan size of 1024x1024 pixels, a dwell time of 20 µs, a probe convergence angle of 10.5 mrad and a camera length of 260 mm. Spectral imaging was performed on selected regions with a scan size of 1024x1024 pixels, a dwell time of 40 µs, and a live time of 8.4 minutes, during which ten frames were recorded. STEM images, spectral images and EDX spectra were acquired using Velox software (Thermo Fisher Scientific). The resulting emd formatted micrographs were converted to TIF format using Velox software.

2.4 Histological staining

To examine the effects of TiO_2-NPs on worm histology, sagittal sections from adult worms exposed to 50 mg/L TiO_2-NPs for seven days were stained with hematoxylin and eosin (HE) (Supplemental A.3). This concentration and exposure duration were chosen since we found effects on stem cells and neuroregeneration (Figure 5, 6). Four control animals and five exposed animals were sectioned and stained. The distribution of acid and neutral mucin was studied in sections of adult worms exposed to 100 and 500 µg/L TiO_2-NPs for three days, as this was the lowest concentration at which increased mucus production was observed. Four animals were

sectioned and stained with Alcian blue and periodic acid–Schiff stain (PAS) per condition to detect mucin (Supplemental A.3).

Digital images for examination were acquired with a Nikon DS-Ri2 camera mounted on a Nikon Eclipse 80i microscope. Sagittal sections through the middle of the pharynx were chosen for standardized comparison of control and exposed animals. The thickness of the mucus layer after Alcian blue/PAS staining was measured using the Fiji image processing package (ImageJ v 1.52n).

2.5 Immunohistochemistry

The mitotic activity of stem cells in response to TiO_2-NPs exposure was determined by immunolabeling of anti-phospho-histone H3 (H3P) (Ser10, 1:1000, Cell-Signaling), as previously described in Pirotte et al. (2015). Samples were digitized microscopically using a Nikon Eclipse 80i fluorescence microscope with a Nikon DS-Ri2 digital camera and the number of mitotic stem cells was counted with Nikon imaging software (NIS-Br). The number of mitotic stem cells was normalized against the total body surface area of the worm. The mitotic activity of stem cells was studied in regenerating heads and tails exposed to five and 50 mg/l TiO_2-NPs at three and 7 dpa. Three experiments were stained at 3 dpa, and two at 7 dpa, all with six samples per condition.

In addition, the effect on the central nervous system was studied by labeling anti-synapsin 3C11 (1:50, Developmental Studies Hybridoma Bank, developed by Buchner E.) as described by Pirotte et al. (2015). A Nikon Ds-Ri2 camera mounted on a Nikon eclipse i80 fluorescence microscope was used for imaging. All measurements were performed with the image processing package Fiji (ImageJ v 1.52n). The relative brain ganglia width was determined by dividing brain ganglia width by head width, as described by Hagstrom et al. (2015). Furthermore, the formation of the anterior commissure was checked. Cephalic brain ganglia regeneration was determined in regenerating tails exposed to 5 and 50 mg/L TiO_2-NPs for seven and 14 dpa, while degeneration was determined in adult organisms under the same exposure conditions. Three experiments were conducted with at least five individuals per condition. One experiment was performed at 9 dpa under the same exposure conditions to follow-up neuroregeneration.

Furthermore, axonal projections of the nervous system were studied using the antibody 1H6-E9 (1:600, Developmental Studies Hybridoma Bank, developed by Zayas, R.M.) (Protocol in supplemental A.4). The expression of 1H6-E9 was determined in at least five regenerating tails,

exposed to 5 and 50 mg/L TiO_2 for seven days in three separate experiments. In addition, an experiment was performed at 9 dpa to confirm these results. Confocal imaging was performed with a Zeiss LSM880 META confocal microscope mounted on an Axiovert 200 M (Zeiss).

2.6 Whole mount fluorescent *in situ* hybridization

The expression of a general stem cell marker (*smedwi-1*) and an early progeny marker (*NB21.11e)* was determined using FISH. In addition, the protocol was used to visualize the cholinergic neurons (*Dj-choline acetyltransferase (ChAT)*). The FISH protocol is based on King and Newmark (2013) and adapted as described by Leynen et al. (2019). To visualize *Smedwi-1* patterns in regenerating heads and tail fragments, the worm fragments were exposed to 5 and 50 mg/L for three and 7 dpa. A fluorescence microscope (Nikon Eclipse 80i) with a Nikon DS-Ri2 digital camera or confocal microscopy (LSM900, Zeiss) was used for imaging for *NB.21.11e* and *Smedwi* respectively. The number of positive cells was counted in heads in the mid-head region, while for regenerating tail fragments, the post-pharyngeal area was used to calculate the average number of cells per animal. Cells expressing *NB.21.11e* were counted using Nikon imaging software (NIS-Br) and normalized against the surface area of the selected location. *Smedwi-1* and *ChAT* data were qualitatively evaluated by looking at the fluorescence intensity and structure of the staining. Three experiments with *Smedwi-1* and two with *NB.21.11e* were carried out, each with at least five individuals per condition.

2.7 Mucus extraction and staining

The mucus production during exposure was quantified on animals that were exposed to 5 and 50 mg/L for three days. An independent experiment with silica nanoparticles and SLS was executed as a control to check if the mucus production was also elevated with a skin irritant and another nanoparticle. The exposure conditions can be found in supplements (Supplement A.5). Therefore, using a cell scraper, the mucus was collected from the bottom of the six-well plate and homogenized by pipetting up and down in the well plate. Then, 1.5 ml of the homogenized mucus was transferred to an Eppendorf tube. This was done in duplicate for each sample. Next, the homogenized mucus was centrifuged for 20 min at 4°C at 10,000 g to create a mucus pellet. After removal of the supernatant, the samples were washed three times with ultra-pure Milli-Q water. Between each washing step, a centrifugation of 10 minutes at 10,000 g at 4°C was done. Subsequently, the pellet was stained with Wheat Germ Agglutinin (WGA) (Alexa FluorTM 488 conjugate of WGA; Thermo Fisher Scientific) for 10 min. The pellet was washed with ultra-pure water three times, with a centrifugation step in between each time. Finally, the

supernatant was removed and 100 µl of ultra-pure water was added to resuspend the pellet. Afterwards, 100 µl of the stained mucus solution was added to a black 96-well plate to measure the fluorescence intensity with a spectrophotometer (FLUOstar Omega, BMG LabTech) at an emission maximum of 519 nm. For each TiO_2-NPs concentration, six measurements were made over two separate experiments.

2.8 Statistical analysis

All data are represented by the average of at least two independent experiments with a minimum of five biological replicates. Statistical analysis for blastema size, cell count, brain width, presence/absence of the anterior commissure, behavioral tests and mucus quantification was performed in the open-source software RStudio 1.2.5033 (Rstudio, Inc.), running R version R 4.0.3 GUI 1.73 Catalina build (R Core Team, 2019). The assumptions of normality and homoscedasticity were checked using the Shapiro-Wilk test and Levene's test, respectively. If the data were not normally distributed, they were transformed with log, 1/x, exp or square root. Next, one-way ANOVA was used and subgroups were compared using Dunnett's post hoc tests. In cases where normality was still not met, a non-parametric alternative was used (Kruskal-Wallis test with pairwise Wilcoxon rank-sum test). *P*-values ≤ 0.05 were considered statistically significant. To check the significance of binomial data (more specifically the presence/absence of the anterior commissure), the Fisher exact test was used.

3. Results

3.1 Characterization of TiO_2-NPs

The average minimum Feret diameter of TiO_2-NPs was 21 ± 8 nm (N = 313) (Figure 2B-C). This corresponds to the manufacturer's specified external dimension of 21 nm. The particle aspect ratio (which is the ratio between the shortest and longest dimension and gives an indication of the elongation of the particle) was 1.216. TEM images showed that TiO_2-NPs had irregular shapes and flattened sides (Figure 2A). Figure 2C illustrates TEM and DLS measurements conducted in ultra-pure water and cultivation medium at a concentration of 5 mg/L. The Z-average measured in ultrapure water was 178 nm, which was 60 nm smaller than the Z-average in the cultivation medium (248 nm). The difference in size between the TEM measurements and the hydrodynamic diameter measured in ultra-pure water suggests an agglomeration of the particles in water. The zeta potential and the polydispersity index measured in cultivation medium containing 5 mg/L TiO_2-NPs were -13.2 mV and 0.25, respectively, indicating an incipient unstable suspension (Figure 2C). DLS measurements of 25

mg/L TiO_2-NPs in cultivation medium in the presence of worms, showed in general a larger hydrodynamic diameter compared with the DLS measurements of 5 mg/L TiO2-NPs in cultivation medium only. During exposure (day 0 - day 3), the Z-average size was 1896 nm at day 0 but declined after two (Z-average = 1078 nm) and three days of exposure (Z-average = 746 nm) (Figure 2D). This indicates that a higher concentration of TiO2-NPs and the presence of worms lead to more agglomeration of the particles, as observed by the zeta potential (-0.92) (Figure 2D). A zeta potential around 0 mV indicates agglomeration of the particles (Tanvir et al. 2015).

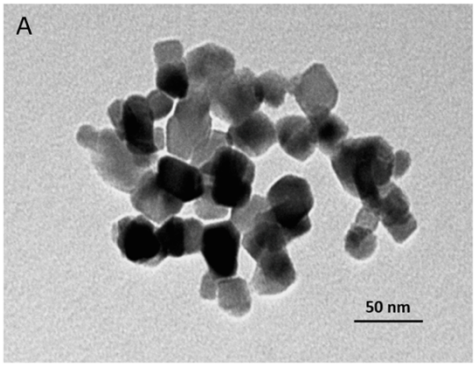

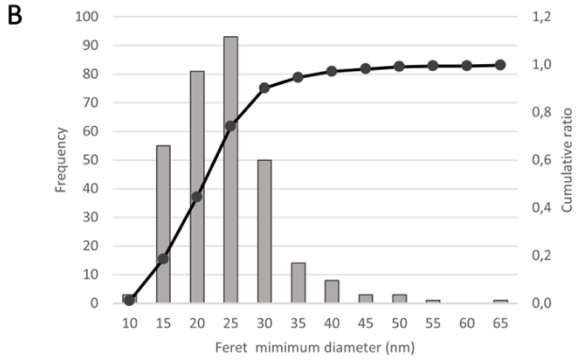

C

	TEM			*DLS*						
	Mean min. feret (nm)	Mean max feret (nm)	Mean ECD (nm)	Hydrodynamic diameter dH (nm) cultivation medium			Z-average ultra-pure water	Z-average cultivation medium	Zeta potential (mV)	PdI
				D10	*D50*	*D90*				
TiO_2 NPs	21 ± 8	27 ± 10	24 ± 8	138.2	247.6	443.8	178	248	-13.20	0.25

D

	DLS					
	Z-average diameter (nm)	**Hydrodynamic diameter (nm)**			**Zeta potential (mV)**	**PdI**
		D10	D50	D90		
Day 0	1896	629	1128	2023	-0.92	0.231
Day 1	1950	1759	1925	2108	/	0.147
Day 2	1078	321	598	1115	-0.38	0.345
Day 3	746	213	402	760	-0.57	0.338

Figure 2: TiO_2-NPs characterization using TEM and DLS. (A) Representative TEM-micrograph of TiO_2-NPs. Scale bar = 50 nm. (B) Histogram with cumulative frequency distributions of particle minimum Feret diameters. (C) The minimum and maximum Feret diameter ± standard deviation and the mean equivalent circle diameter (ECD) ± standard deviation was measured by TEM (N = 313). The volume-based (mean) hydrodynamic diameters, zeta-potential (mV) and polydispersity index (PDI) of 5 mg/L TiO_2-exposure

385 medium or ultra-pure water were measured by DLS. The volume-based D10, D50 and D90
386 correspond to the 10%, 50%, and 90% of particles under the reported hydrodynamic diameter.
387 (D) Hydrodynamic diameters after the addition of 25 mg/L exposure medium to worms at day
388 0, day 1, day 2 and day 3 after the start of the exposure. The table shows intensity-based Z-
389 average sizes, volume-based D10, D50 and D90 and zeta potentials.
390
391 3.2 Uptake of TiO_2-NPs through the epidermis and intestine of *S. mediterranea*
392 HAADF-STEM imaging and EDX analysis on tissue sections of exposed animals revealed
393 TiO_2-NP agglomerates in the epidermis, gut wall, and in the parenchymal tissue between the
394 epidermis and gut (Figure 3A, 3C). Particles were also found in the gut cavity (Supplement Fig.
395 B.2). Most TiO_2-NPs were observed on the ventral side of the animal, mainly in the mucus
396 layer (Supplement Fig. B.2). When TiO_2-particles were injected into the intestine, uptake via
397 the intestine was observed (Figure 3B).
398
399 3.3 TiO_2-NPs exposure results in an altered epidermal structure and increased epidermal mucus
400 production
401 The planarian epidermis is characterized by a structured monolayer composed of columnar
402 cells, recognizable by large nuclei and rhabdites, which are unpigmented (Rompolas et al. 2009)
403 (Figure 4A). Animals exposed to 50 mg/L TiO_2-NPs had disorganized epidermal tissue on the
404 dorsal side (Figure 4A). However, no ultrastructural effects were found in the dorsal epidermis.
405 In the intestine, no morphological alterations were detected after histological examination.
406 An increase in mucus deposition was observed in both adult and regenerating worms that were
407 exposed to 25 and 50 mg/L. This was already visible from the first day of the exposure (day 0)
408 (Supplement Fig. B.3). Furthermore, the quantification of the mucus production with WGA,
409 also showed an increase at 50 mg/L. The skin irritant sodium lauryl sulphate (SLS) was used
410 as a positive control (Supplement Fig. B.4). In addition, comparable observations were noted
411 following exposure to silica nanoparticles (Supplement Fig. B.4), suggesting a potentially
412 common epidermal irritation effect by nanoparticles.
413 The thickness of the mucus layer was studied using an Alcian blue/PAS. We observed a
414 concentration-dependent increase in epidermal mucosal thickness in the exposed group (Figure
415 4A, AB). No changes in mucus secretion were observed in the ventral epidermis or in the gut.
416

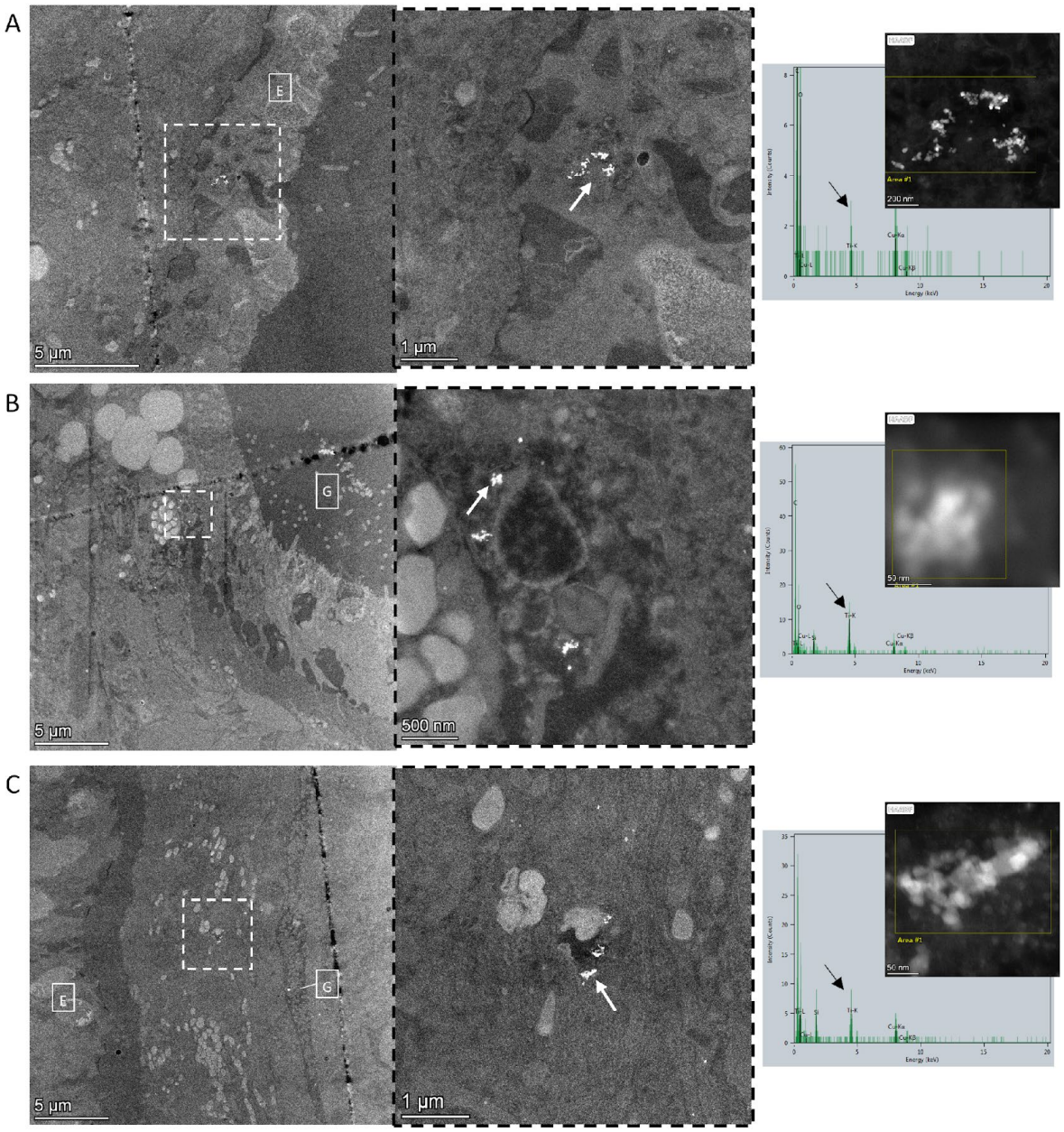

Figure 3: Localization of TiO_2-NPs in tissues by HAADF-STEM. Overview images of TiO_2-NP agglomerates in worm tissues, with the area of enlargement indicated with dashed squares. The presence of TiO_2-NPs is indicated with arrows and the corresponding EDX elemental analyses are shown. (A) TiO_2-NPs in the epidermis in a regenerating tail exposed to 50 mg/L TiO_2 for seven days, (B) TiO_2-NPs outside the gut cavity in TiO_2-injected adult worm exposed for three days, and (C) TiO_2-NPs located in between the epidermis and the gut cavity in a tail exposed to 50 mg/L TiO_2 for seven days. Abbreviations: epidermis (E), gut cavity (G).

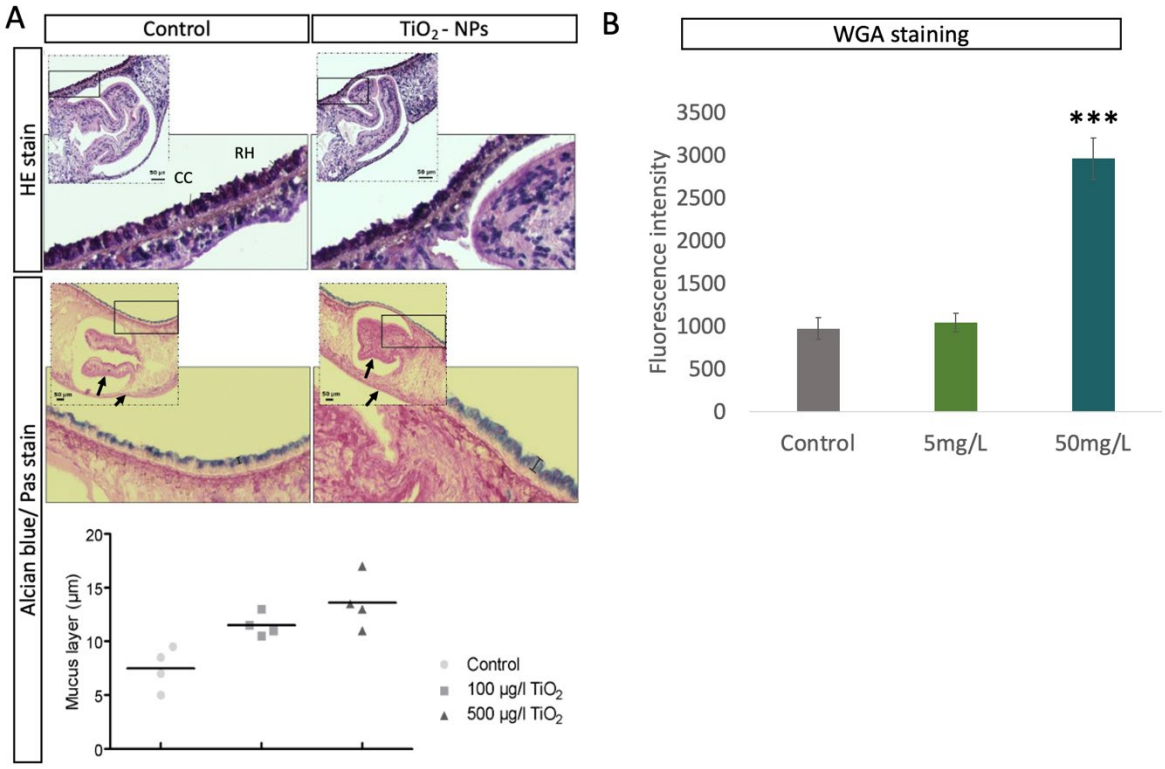

Figure 4: Visualization and quantification of the mucus production after exposure to TiO_2-NPs. (A) Sagittal sections taken through the pharynx and stained with x and y were analysed. The region of enlargement is shown by a black square. Scale = 50 µm. HE stains revealed morphological alterations of the dorsal epidermis after seven days of exposure to 50 mg/L TiO_2. In the epidermis of control worms, rhabdites (Rh) and columnar cells (CC) are visible. The figure shows representative images based on an experiment containing two control worms and four exposed worms. The mucus layer thickness (µm) stained via the Alcian blue/PAS stain is plotted for each TiO_2 concentration (0, 100 and 500 µg/L) after three days of exposure. The ventral mucus layers are indicated with an arrow, while the intestine is indicated with a diamond arrow. The mean thickness of the mucus layers corresponds to 7.5 µm for the controls, 11.5 µm for 100 µg/L TiO_2 and 13.6 µm for 500 µg/L TiO_2. The graphs summarise the results of four animals per condition. (B) Mucus measurements using spectrophotometry for controls, 5 mg/L and 50 mg/L TiO_2-NPs exposed animals. The mucus was stained using WGA and intensity was measured at 519 nm after three days of exposure as a representation for the amount of mucus produced. Mucus was measured in six samples of each condition over 2 separate replicates. Statistical significance relative to control is indicated by: ***: $p \leq 0.001$.

3.4 TiO_2-NPs impair neuroregeneration

To investigate neurotoxicity and the impact of TiO_2-NPs on neuroregeneration, planarian behavior, eye development, and the structure of the nervous system were monitored The behavior of regenerating worms was influenced by TiO_2-NPs. Specifically, regenerating heads exposed to 50 mg/L TiO_2-NPs showed a dragging behavior, starting 2 dpa and continuing until 4 dpa. At 5 dpa, this aberrant behavior was not present anymore. Regenerating tails showed side-lying behavior, which was observed between three and 8 dpa. After 7 dpa, the motility and light avoidance tests showed no significant differences between control and exposed worms (Supplement Fig. B.5). Underlying to this, in regenerating worms exposed to 5 mg/L and 50 mg/L, eye regeneration was unaffected at 7 dpa (Figure 5A). At this time point, the tails exposed to 50 ml/L TiO2-NPs were regenerating the brain ganglia, but lacked the anterior commissure (AC) in 38% of the animals, compared to the unexposed worms (Figure 5D). At 9 dpa, only 25% of the worms exposed to 50 mg/L TiO_2-NPs were able to form the AC. No effects on relative brain width were noticed (Supplement Fig. B.6A), nor were adverse effects detected on the axonal projections at 7 dpa and 9 dpa (Figure 6C). At 14 dpa, all tails exposed to 50 mg/L TiO_2-NPs regenerated an AC and showed no difference in brain width (data not shown). In addition, no differences in the formation of the cholinergic neurons were observed between the controls and the group exposed to 5 mg/L for seven days (Supplement Fig. B.6C). In adult worms, no effects on the relative brain widths or the ventral nerve cords were observed when stained with anti-synapsin (Supplement Fig. B.6A-C). The anterior axonal projections (1H6) (Figure 5C) of exposed adult worms and the cholinergic neurons (ChAT) were also unaffected (Supplemental fig. B.6).

3.5 TiO_2-NPs cause a cell cycle delay

Tissue regeneration and stem cell dynamics were studied at 3 (Figure 6A-C) and 7 (Figure 6D-F) dpa. None of the tested TiO_2-NPs concentrations affected tissue growth at 7 dpa (Supplement Fig. B.7). There were no discernible effects in the pattern of stem cells (*Smedwi 1*) at 3 or 7 dpa (Figure 6A, 6D). At 3 dpa, the number of proliferating stem cells (H3P) in tails exposed to 5 mg/L TiO_2-NPs was significantly increased ($p \leq 0.01$) (Figure 6B), but there was no effect on the stem cell progeny number (*NB21.11e*) (Figure 6C). At 7 dpa, stem cell proliferation was significantly reduced in tails exposed to both 5 and 50 mg/l TiO_2-NPs ($p \leq 0.001$). The stem cell progeny content in heads exposed to 50 mg/L TiO_2-NPs was significantly lower at 7 dpa ($p \leq 0.01$) (Figure 6F). However, after 14 days, no significant effects were seen in stem cell

proliferation in regenerated head and tail fragments after exposure to 5 mg/L, implying that regeneration is delayed but not impaired (Supplement Fig. B.8).

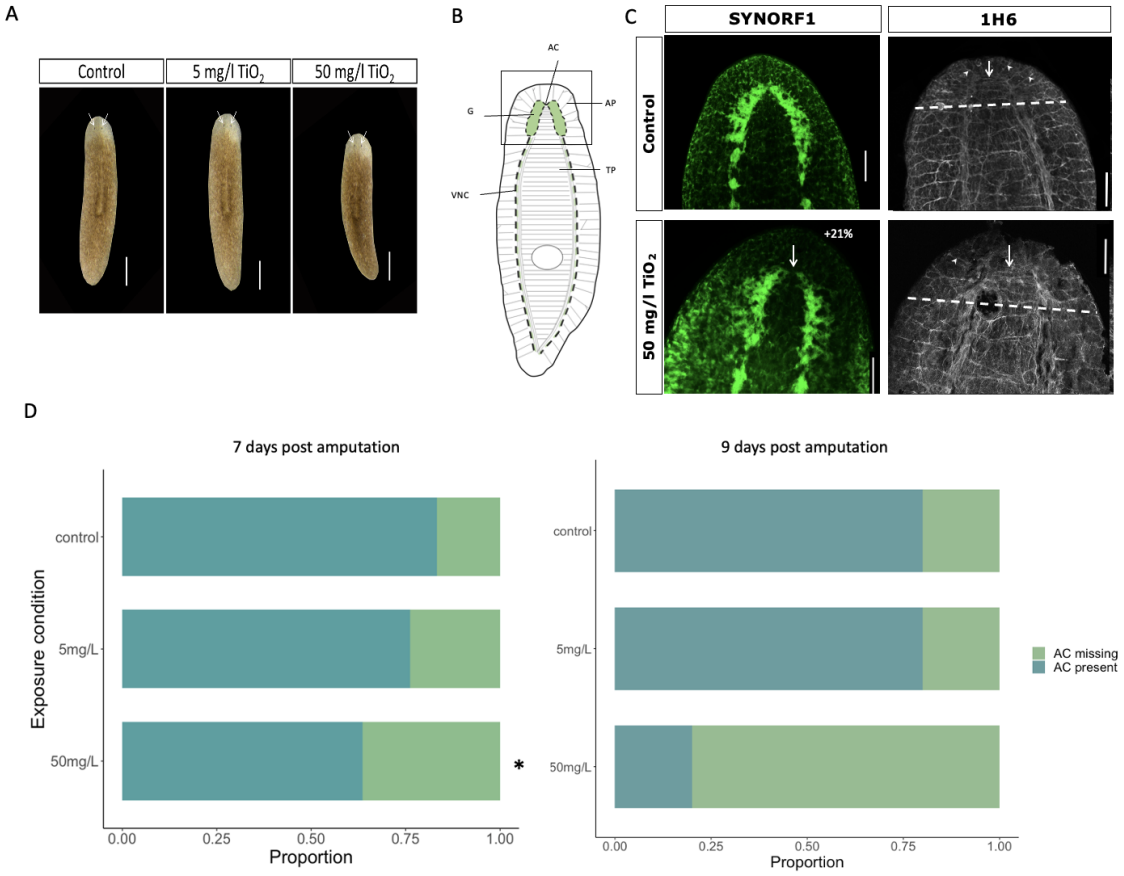

Figure 5: Effects on nervous system regeneration after exposure to TiO_2-NPs. (A) Representative images of regenerated photoreceptors (indicated by arrows) in control, 5 mg/L TiO_2 and 50 mg/L TiO_2 exposed tails at 7 dpa. Scale bars = 500 µm. (B) Overview of nerve structures stained with anti-synapsin (ventral nerve cords (VNCs), ganglia (G) and anterior commissure (AC), dashed lines) and anti-1H6-E9 (VNCs, transverse and anterior projections (TP, AP), solid lines). (C) The formation of the anterior commissure in tails that are regenerating a new brain during exposure to 5 mg/L and 50 mg/L TiO_2 (arrows). Pooled results of three independent experiments, with a total number of replicates of ≥ 13 tails per condition. Staining anti-1H6-E9 showed no differences between tails of different conditions. Results from one experiment, with six tails per group. Scale bars = 50 µm. (D) The proportion of regenerating tails that developed an anterior commissure (AC) at 7 dpa and 9 dpa. Pooled results of three independent experiments with at least 15 tails per condition at 7 dpa and one experiment at 9 dpa with five tails per condition. Statistical significance relative to control is indicated by: *: $p \leq 0.05$.

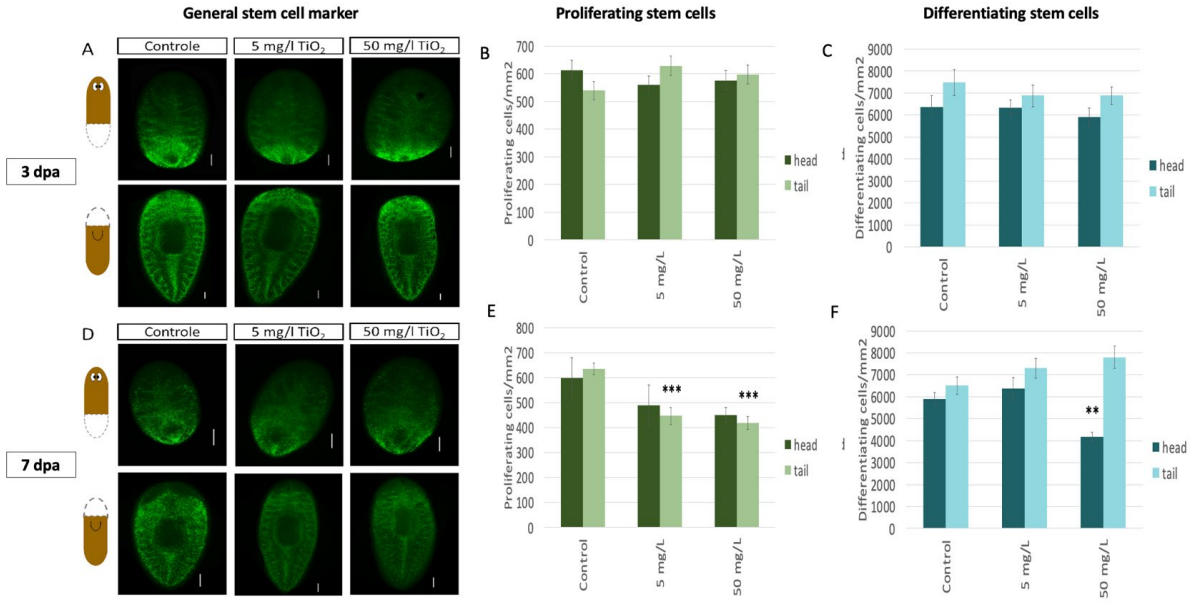

Figure 6: Effect on stem cell dynamics after exposure to TiO_2-NPs. Animals were cut and exposed to 5 and 50 mg/L TiO_2 for three days (top figures) or seven days (bottom figures). Stem cell dynamics were investigated by a combination of different parameters. (A) *Smedwi-1 expression* (general stem cell marker) in 3 dpa fragments, scale bars = 250 µm. Representative images of three independent experiments, with a total of ≥ 14 samples per condition. (B) H3P-positive cells (proliferating stem cells) in 3 dpa fragments. The graphs represent the results of three independent experiments, with a total of ≥ 21 samples per condition. (C) *NB21.11e*-positive cells (a proxy for differentiating stem cells in 3 dpa fragments). The graphs represent two independent experiments, with a total of ≥ 10 samples per condition. (D) *Smedwi-1 expression* in 7 dpa fragments, scale bars = 250 µm. Representative images of two independent experiments, with a total of ≥ 11 samples per condition. (E) H3P-positive cells in 7 dpa fragments. The graphs represent two independent experiments, with a total of ≥ 8 samples per condition. (F) *NB.21.11e*-positive cells in 7 dpa fragments. The grapsh represents two independent experiments, with a total of ≥ 10 samples per condition. Statistical significance relative to control is indicated by: **: $p \leq 0.01$; ***: $p \leq 0.001$.

4. Discussion

Research on the toxicity of titanium dioxide nanoparticles (TiO_2-NPs) in the marine aquatic environment has received significant attention in recent years, as emphasized by Huang et al. (2018). Despite this, the current risk assessment framework lacks a comprehensive understanding of the impact of TiO_2-NPs on organisms in all types of aquatic compartments,

often ignoring developing organisms, and containing a lot of variation in the reported effects. Addressing these gaps, our study investigates the effects of TiO_2-NPs on the epibenthic invertebrate *S. mediterranea*. The reported variation was addressed by integrating aspects of nanoparticle uptake, their characteristics, and the subsequent adverse effects observed in both adult and developing organisms. Past research has often documented diverse effects attributed to differences in particle type and concentration, or specific to the organism under study. We used spherical P25 aeroxide TiO_2-NPs with a diameter of 21 nm, a TiO_2-NP type that is widely used on the market because of its photocatalytic properties (Boutillier et al. 2020).

Our data shows that particle characteristics changed with altered particle concentrations and the amount of biological material (Figure 2). Agglomerates were most likely formed when particles were trapped by mucus released by the worms, leading to particle sedimentation. The agglomeration of cerium nanoparticles due to mucus was also seen in the human 3D airway model systems (Kuper et al. 2015), where both the agglomeration and aggregation increased when respiratory mucus was added to the model system. In aquatic models and ecosystems, agglomeration and subsequent sedimentation of nanoparticles enable the uptake of particles by benthic organisms (Dube and Okuthe 2023). In our study, this resulted in the ingestion of sedimented particles through the ventral pharynx (planarian mouth) (Supplement Fig. B.2D), although absorption via the epidermis was also observed. Epidermal uptake was mainly observed on the dorsal side. On the ventral side, the particles were trapped between the cilia and the mucus (Supplement Fig B.2B-C). From previous research, we know that TiO_2 particles of different sizes (ranging from 21 to 100 nm) end up in different tissue (Ramsden et al. 2009, Hu et al. 2018). In rainbow trout, an accumulation of TiO_2 particles was seen in the gill, gut, spleen, liver, and brain (Ramsden et al. 2009). Similarly, in *C. elegans* TiO_2 particles were found in the cytoplasm of primary neurons (Hu et al. 2018). In our study, we mainly observed intracellular TiO_2 - NPs in the gut, epidermis, and parenchymal tissue of the planarians (Figure 3).

Planarians respond to epidermal exposure, and resulting irritation, by increasing mucus secretion (Oliveira et al. 2018). This was demonstrated at different concentrations and exposure times (Figure 4). Consequently, adult worms exposed to TiO_2-NPs concentrations greater than 0.1 mg/L had a dorsal mucus layer 1.5 times thicker than the control animals (Figure 4A). On one hand, the increase in the formation of mucus will protect the planarians, as also shown in Foraminifera, which not only formed mucus when exposed to titanium dioxide nanoparticles but also excreted nanoparticles encapsulated in mucus (Ishitani et al. 2023). On the other hand,

554 the excreted and trapped particles increase the risk of intestinal uptake. However, in contrast to
555 previous studies, no obvious morphological or (ultra)structural changes were observed in the
556 gut, even after direct injection of TiO_2-NPs (Supplement Fig. B.2D). In zebrafish, TiO_2-NPs
557 (200 and 400 µg/g food) disrupted the intestinal epithelium (*Danio rerio*) by rupturing the lining
558 of the epithelial cells of intestinal villi after feeding fish food-laced with a mineral UV filter
559 containing TiO_2 (30% NP) (da Cunha and de Brito-Gitirana 2020). In mice, the colonic
560 epithelium was injured after seven days of oral exposure to 1 mg/kg/day 25 nm anatase TiO_2-
561 NPs (Li et al. 2019). As indicated before, these differences can be attributed to the difference
562 in exposure route (feeding vs. water), exposure concentration and particle size.
563
564 During TiO_2-NPs exposure planarians dragging and side-lying, albeit without severe
565 neurodegenerative impairments (Supplement Fig. B.5). Neurogenesis, on the other hand, was
566 affected, as a significant number of regenerating tails exposed to 50 mg/L TiO_2-NPs were
567 missing their anterior commissure at 7 dpa and 9 dpa (Figure 5D). The anterior commissure is
568 the largest commissure in the planarian CNS, connecting the two lobes of the cephalic ganglia,
569 and is the crossing place for many axons (Roberts-Galbraith et al. 2016). Normally, anterior
570 commissure regeneration and consequent cephalic ganglia lobe reconnection start at 3 dpa, and
571 photoreceptor axons cross the midline at the anterior commissure (Ross et al. 2017). TiO_2-NPs
572 did not affect the regeneration of the eye pigment cells at 7 dpa (Figure 5A), but it is possible
573 that without the anterior commissure, eye functionality may not be fully restored, explaining
574 the observed behavioral effects (dragging and side-lying behavior). As axonal projections were
575 still able to regenerate but seemed less numerous than in the controls (Figure 5C), and as the
576 anterior commissure fully regenerated after 14 days of exposure to 5 mg/L, we hypothesize that
577 neuroregeneration is probably not permanently impaired, but rather delayed. In zebrafish (*D.*
578 *rerio),* the exposure to TiO_2-NPs (20 nm) also had a negative effect on neurogenesis and motor
579 neuron axon length (Gu et al. 2021), whereas in mice, neurodevelopmental effects were shown
580 in developing offspring after maternal exposure to 1, 2 or 3 mg/kg TiO_2- NPs (6.5 nm) (Hong
581 et al. 2018). Underlying these neuronal effects, Wu et al. (2010) showed that the G2/M phase
582 was disturbed after TiO_2-NPs (20 nm) exposure in dopaminergic neurons, followed by
583 oxidative stress-induced apoptosis. In zebrafish, sub-chronic exposure to TiO_2-NPs and
584 neuronal apoptosis was linked to an over-proliferation of glial cells (Sheng et al. 2016). In our
585 study, impaired neuroregeneration was accompanied by a decrease in stem cell proliferation
586 but no large differences in general stem cell amounts (*Smedwi 1*) were observed (Figure 6),
587 indicating a cell cycle delay. Cell cycle delay was also seen after exposure to other types of

nanoparticles, including silver and plastic particles (Lee et al. 2019, Gao et al. 2022). More research into the potential interference of TiO_2-NPs with the cell cycle in planarians is needed to further link physicochemical particle characteristics and induced modes of action.

5. Conclusion

Our study indicates that TiO_2-NPs exert adverse effects on (neuro)development in the epi-benthic organism *S. mediterranea*. Increased mucus production, as a result of a defense mechanism against irritation, resulted in uptake through both the intestine and the epidermis. In developing tissues, neurodevelopment was affected, characterized by a delay in the anterior commissure regeneration. Underlying stem cell dynamics were disturbed, especially in tail fragments the stem cells in the proliferation phase were affected. Overall, our study shows that developing organisms might be more sensitive than adult organisms to TiO_2-NPs exposures. Hence, we advocate for the inclusion of developing organisms in future risk assessment strategies.

Supplements

A. Supplemental materials and methods

A.1 Particle characterization: TEM analyses

The particles were characterized by quantitative TEM analysis. The procedure to quantify these particles is described here. A region of interest was selected for all images. The constituent particles were analyzed using the watershed mode in the ParticleSizer software, with an irregular watershed convexity threshold of 1 to split up agglomerates. The object-to-background was set at 70 to subtract the background. All other settings were used in default mode. Based on visual inspection, particles at the border of the region of interest, particles with a deviant morphology, and agglomerates were considered artefacts and were excluded from the analysis. Distributions of short axis length (minimum Feret (Feret min)), long axis length (maximum Feret (Feret max)), equivalent circular diameter (ECD) and aspect ratio were determined for at least 100 particles, allowing for an accurate determination of the particle size distribution.

A.2 Fixation protocol TEM

The fixation for TEM was done in 2.5% glutaraldehyde in 0.1 M sodium cacodylate buffer for three hours. The samples were then rinsed twice in sodium cacodylate buffer for 20 minutes, and post-fixed in 2% osmium tetroxide in sodium cacodylate buffer for one hour. Following

the post-fixation, the samples were rinsed twice for 30 min in sodium cacodylate buffer and dehydrated in an ascending series of acetone: 30 min 50%, 45 min 70% and 90%, two times 30 min 100%, and finally 30 min acetone absolute. Next, the samples were impregnated overnight in a 1:1 acetone/Spurr mixture. The next morning 100% Spurr was added and the samples were dried to allow the acetone to evaporate. Fresh Spurr was added for overnight incubation. Finally, the samples were polymerized in Spurr at 70°C for 24 hours. Epoxy-resin embedded samples were cut cross-sectionally into 120-nanometre sections using a Leica Ultracut UCT ultramicrotome and mounted on copper grids (120 mesh).

A.3 Alcian blue/ PAS and HE staining protocol

Samples were fixed in freshwater Bouin's fixative for three hours and dehydrated in an ascending series of ethanol: 75% EtOH, 80% EtOH, 90% EtOH, 96% EtOH, and two times 100% EtOH. Next, the samples were incubated in 1:1 EtOH/butanol, 100% butanol, 100% butanol/paraffin and 100% paraffin. They were embedded in paraffin and 8 µm thick sections were cut and collected on glass slides. Next, the sections were gradually deparaffinized to dH_2O by first washing with xylene (three times) and then in a descending series of ethanol: 100% EtOH (2x), 96% EtOH, 90% EtOH, 75% EtOH and 50% EtOH, each for 15 min. Finally, the samples were submerged in dH_2O for 10 min and then stained.

For HE staining, the deparaffinized sections were submerged in Hematoxylin Erhlich (10 – 20 min) and rinsed under running tap water for 20 min. Next, they were stained with 2% Eosin for 8 – 15 min. The sections were dehydrated in an ascending series of ethanol: 50%, 75%, 80%, and 90% EtOH (a few seconds each), followed by 96% EtOH (10 min) and 100% EtOH abs (two times 15 min). Finally, the sections were submerged twice in xylene for 20 min and mounted in depex.

For mucin evaluation, the sections were incubated in Alcian blue (1% Alcian blue in 3% acetic acid, $1 < pH < 2$) for 30 min and rinsed with dH_2O (5 min). Next, the sections were oxidized in 1% periodic acid (10 min) and rinsed three times in dH2O. They were incubated in Schiffs reagent (0.5% pararosalinin, 0.5% K_2SO_2, 0.3% Norit) for 15 min and rinsed three times with sulphatic water for two min. Finally, they were rinsed in tap water for 15 min and covered with a coverslip.

A.4 Protocol 1H6-E9 staining

The 1H6-E9 staining protocol started by adding 5% N-acetyl-L-cysteine dissolved in PBS to the worms for five minutes. Next, the samples were rinsed in PBS and fixed in 4%

formaldehyde diluted in PBST (0.3% triton) for 15 minutes, and washed twice in PBST. A preheated reducing solution (50 mM dithiothreitol, 1% NP-40 (v/v) and 0.5% sodium dodecyl sulphate) was then added for seven minutes while incubating at 37°C. Samples were rinsed shortly in PBST and treated with 50% MeOH in PBST for five minutes, followed by 100% MeOH (five minutes + one-hour incubation at -20°C). The samples were bleached overnight in 6% H_2O_2 in MeOH under a cold light source. The next day, the worms were rinsed twice in 100% MeOH, followed by 50% MeOH in PBST and subsequently PBST, each for five min. Worm tissue was permeabilized in 2 µg/ml proteinase K solution for seven minutes (in 0.1% sodium dodecyl sulfate in PBST). The samples were post-fixed in 4% formaldehyde in PBST for ten minutes and then rinsed in PBST. Next, the samples were blocked in 1% Bovine Serum Albumin dissolved in PBST for two hours and the primary antibody was added overnight at 4°C. The next day, the samples were rinsed with PBST and subsequently the secondary antibody, Alexa Fluor 488-conjugated Goat Anti-mouse IgG (1:400, Invitrogen), was added overnight. After staining, the samples were rinsed in PBST and mounted in Shandu Immu-mount (Thermo Fisher Scientific).

A.5 Exposure positive controls mucus production experiments

To assess whether mucus production was elevated by other nanoparticles, an experiment using silica nanoparticles was executed. A stock suspension of silica nanoparticles of 19 nm was prepared by dispersing the NPs in ultrapure water to a concentration of 1 g/l, followed by sonication for two times 5 min (probe sonicator, Analis, amplitude 18 mm). In between the cycles, the suspension was put on ice to reduce the temperature increase caused by the sonication procedure. The stock suspensions were stored at room temperature and used within a week. Exposure media were prepared via sonication of the SiO2-NPs stock suspension for 5 min before dilution in planarian cultivation medium. Next, exposure media were sonicated for 30 minutes, to reduce aggregates. Adult animals were exposed to 50 mg/l and 100 mg/l, SiO_2-NPs for three days. Afterwards, mucus was quantified using the protocol described in 2.7 (Mucus extraction and staining).

As a positive control, the skin irritation compound sodium lauryl sulphate (SLS) was used in the mucus production assays. An SLS exposure solution of 0.01% and 0.1% were prepared in planarian cultivation medium. Adult planarians were exposed for 30 seconds to 0.01% SLS and 3 minutes to 0.1% SLS.

B. Supplemental figures

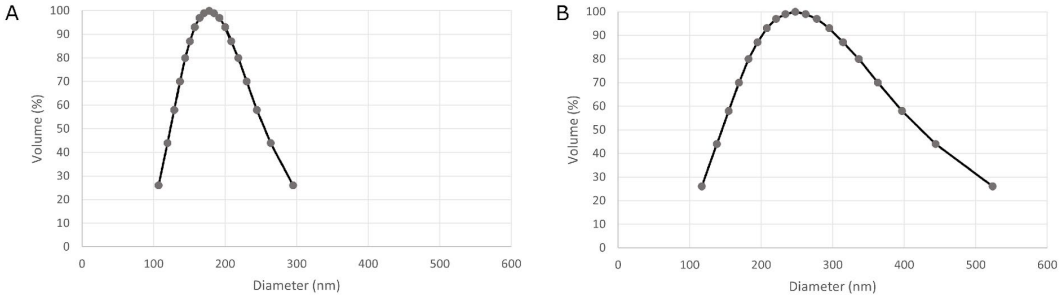

Fig. B.1: Hydrodynamic diameters measured by DLS for particle characterization. Graphs show volume (%) of each diameter (nm) of (A) Stock suspension of 25 mg/l TiO_2-NPs, median hydrodynamic diameter = 178 nm and (B) Exposure medium with TiO_2-NPs diluted in cultivation medium (5 mg/l), median hydrodynamic diameter = 248 nm.

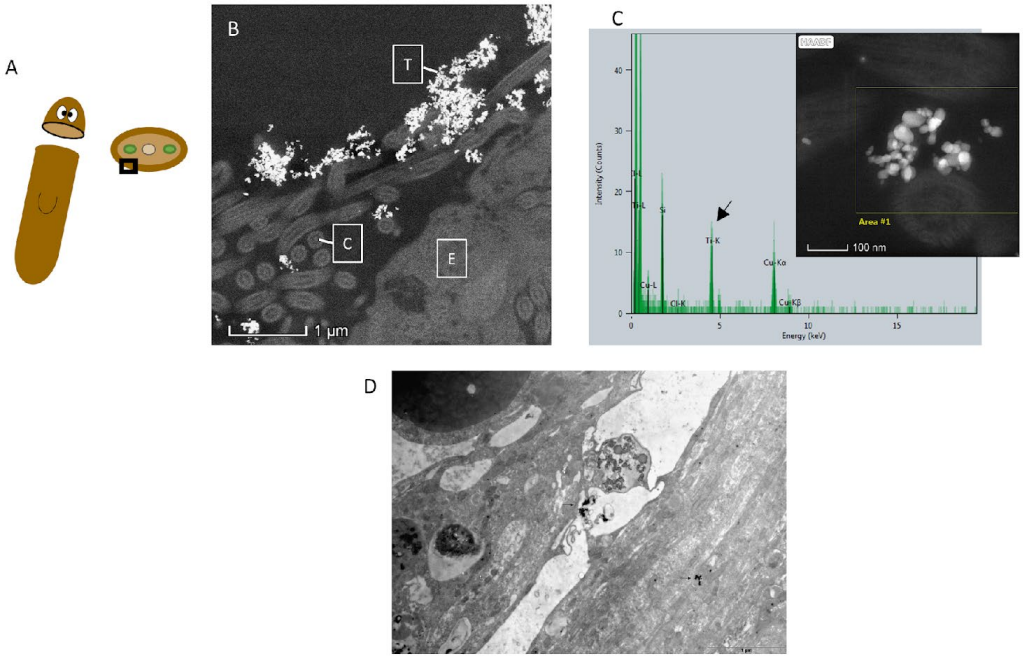

Fig. B.2: TiO_2-NPs uptake and localization in worm tissue. (A) Indication of the location of the studied tissue section in the worm. (B) Accumulation of TiO_2-NP agglomerates at the ventral epidermis, acquired by HAADF-STEM. T = TiO_2, C = cilia, E = epidermis. (C) Corresponding EDX elemental analysis of (B). (D) TEM micrograph of TiO_2-particle (arrows) uptake in and next to the gut cavity of a tail part, exposed to 50 mg/L TiO_2 for seven days.

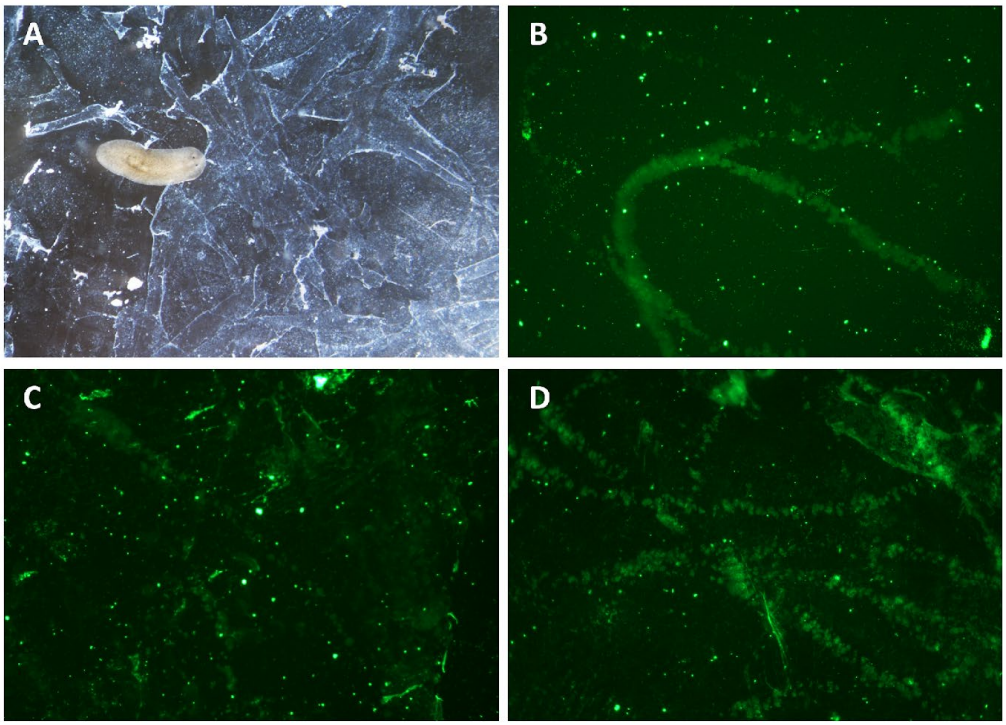

Fig. B.3: Mucus precipitation after TiO_2 exposure. Representative images of mucus precipitation at the bottom of the wells. (A) Visually after one day during a 25 mg/L TiO_2-exposure, or stained with WGA, with worms exposed for three days to (B) 0 mg/L TiO_2 (control), (C) 5 mg/L TiO_2 and (D) 50 mg/L TiO_2. All conditions showed mucus precipitation and mucus trails, which increased in number with TiO_2 concentration.

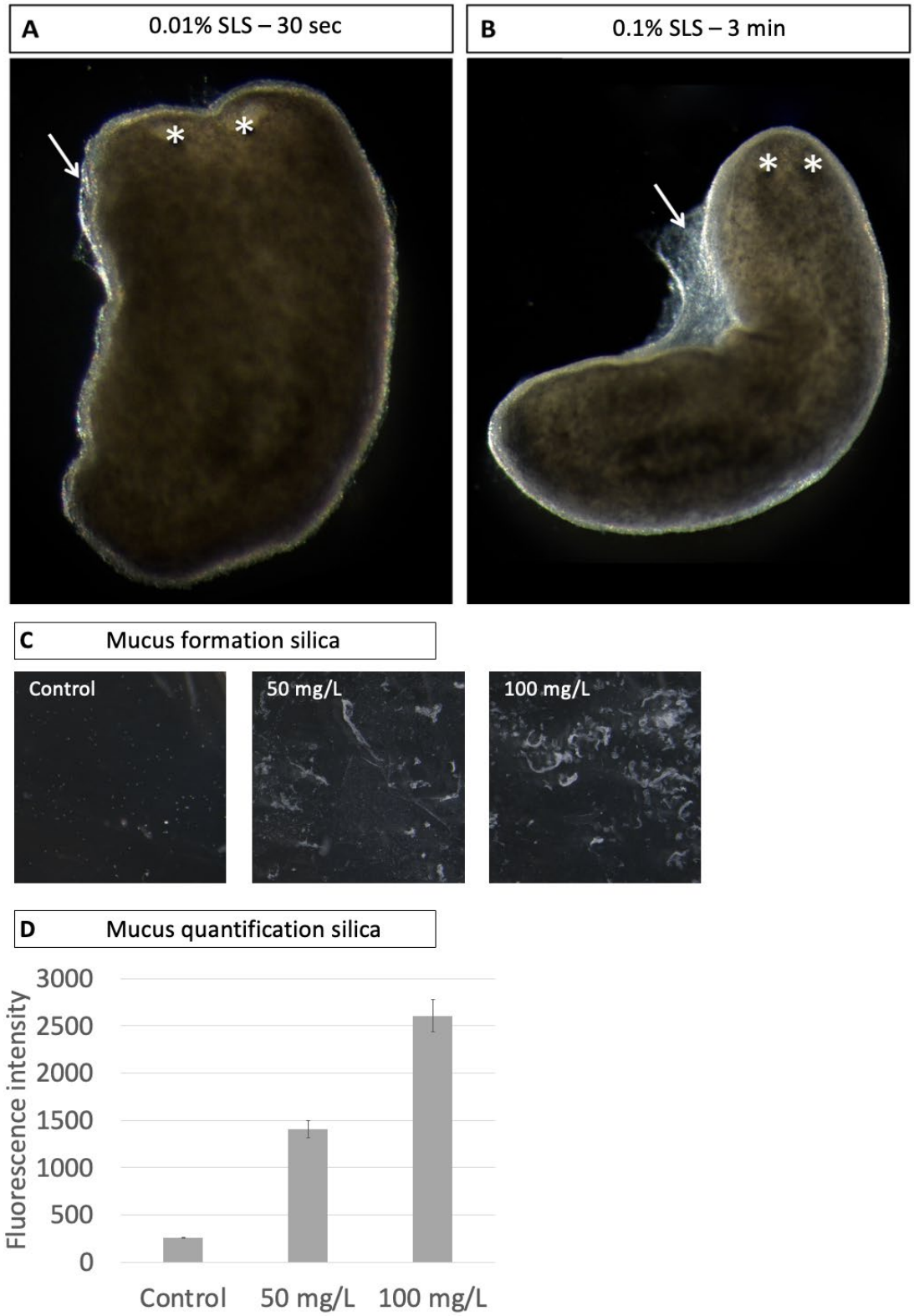

711

712 **Fig. B.4: Epidermal mucus formation in response to known irritating compounds**.
713 Exposure of planarians to an irritant compound result in increased epidermal mucus production.
714 (A) 30 sec of incubation in 0.01 % sodium lauryl sulphate (SLS) induces a small increase in
715 mucus production while (B) three min incubation in a higher concentration of 0.1 % SLS

increases mucus production substantially. The asterisks indicate the positions of the eyes in the animals. (C) Mucus secretion during exposure to 20 nm synthetic SiO_2-NPs at 0 mg/l (Control), 50 mg/l, and 100 mg/l. Mucus is visible as white flakes. (D) Mucus measurements using spectrophotometry for controls, 50 mg/L and 100 mg/L SiO_2-NPs exposed animals. The mucus was stained using WGA and intensity was measured at 519 nm after three days of exposure. Mucus was measured in five samples of each condition over 1 replicate.

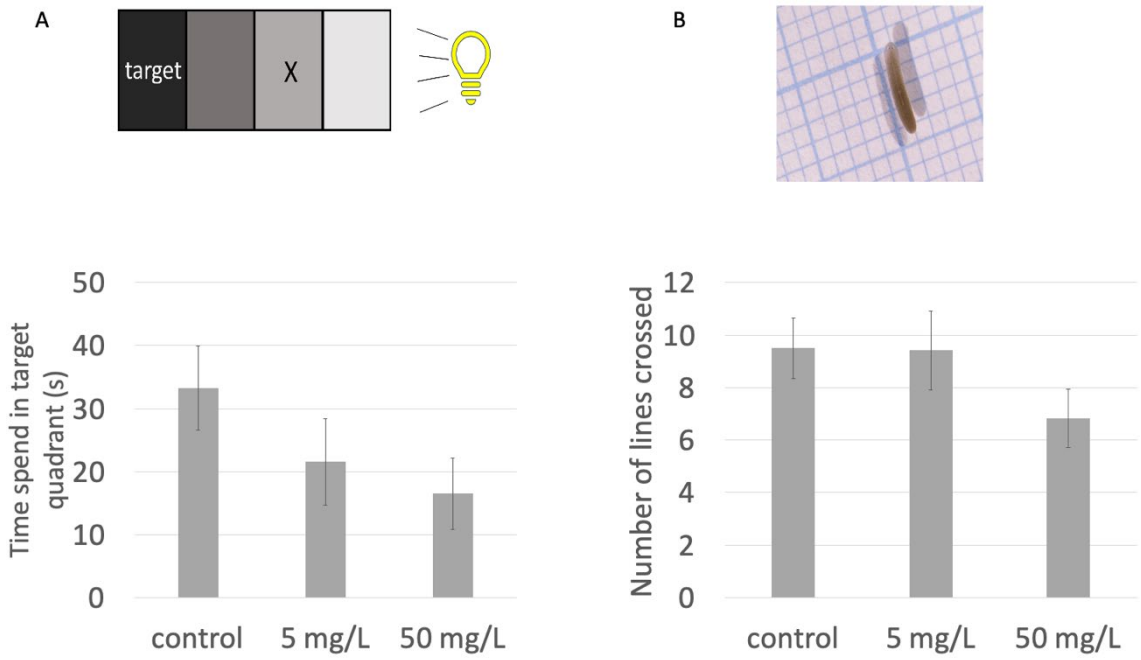

Fig. B.5: Experimental setup and results of the behavioral assays after exposure to TiO_2-NPs. Tail parts were subjected to (A) a light avoidance test (negative phototaxis) and (B) a speed analysis, after exposure to 50 mg/L TiO_2-NPs at 7 dpa. A schematic overview of the light avoidance test is shown, with the container exposed to a cold light source from the front side, ensuring a gradient in light intensity. The target quadrant was the darkest region, and worms were placed in the box at the X at the start of the experiment. The negative phototaxis was measured as the time spent in the target quadrant within a timeframe of 1m40s. The speed analysis was measured as the number of lines of 0.5 cm crossed within a timeframe of 1m40s. Results of four experiments, with at least 11 replicates per condition.

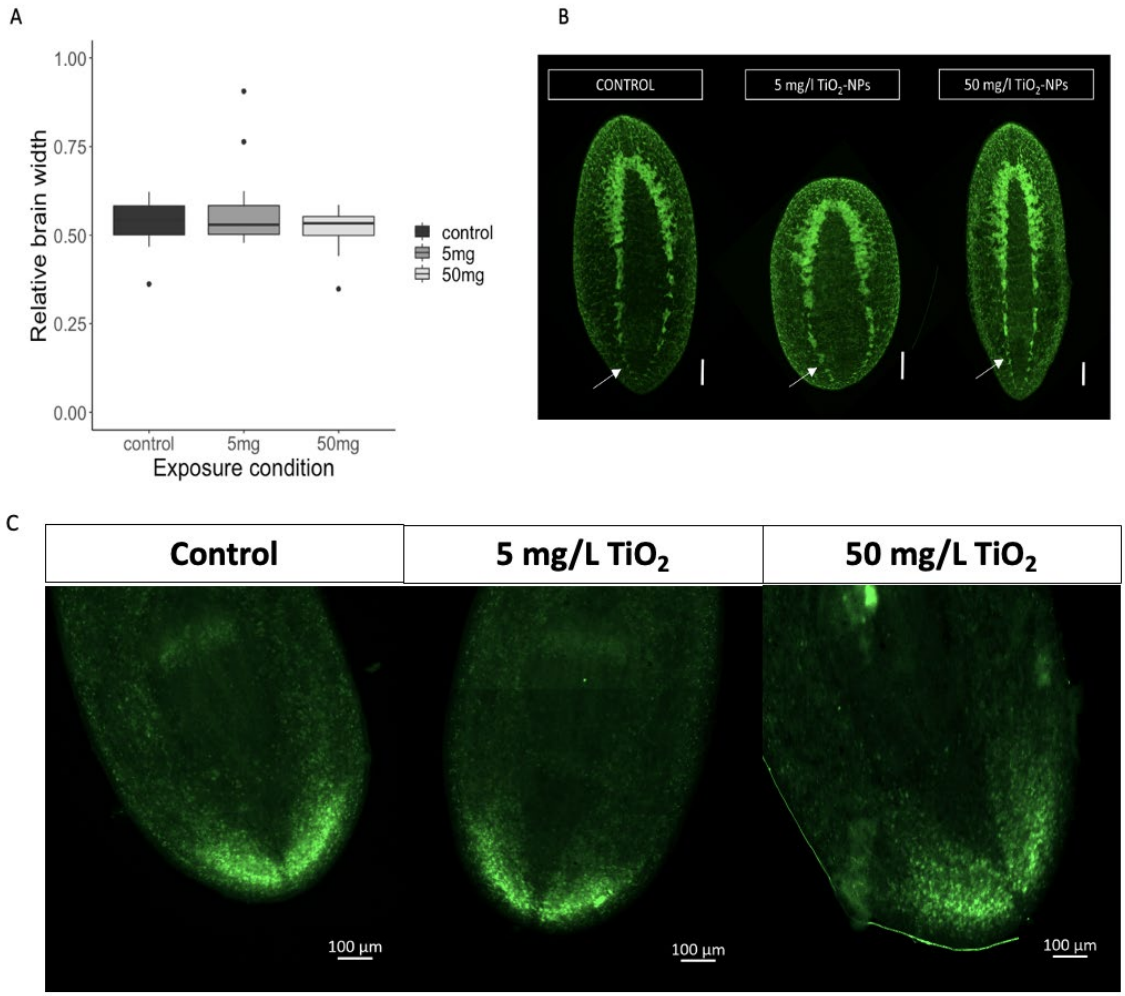

734

735 **Fig. B.6: Neuroregenerative defects after exposure to TiO_2-NPs.** (A) Relative brain widths
736 of tail parts at 7 dpa, after regenerating in 5 and 50 mg/L TiO_2. Control = 0.538, 5 mg/l TiO_2 =
737 0.630 and 50 mg/l TiO2 = 0.519. Results of three independent experiments, with a total number
738 of replicates of ≥ 15 samples per condition. (B) Nerve cord regeneration of head parts at 7 dpa,
739 after exposure to 5 and 50 mg/L TiO_2. Scale bars = 100 µm. The arrow indicates the formation
740 of the nerve cords in the tail parts. (C) Visualisation of the cholinergic neurons of the tail parts
741 after 7 dpa, after exposure to 5 mg/L TiO_2 and 50 mg/L TiO_2. Scale bars = 100 µm.

742

743

744

745

746

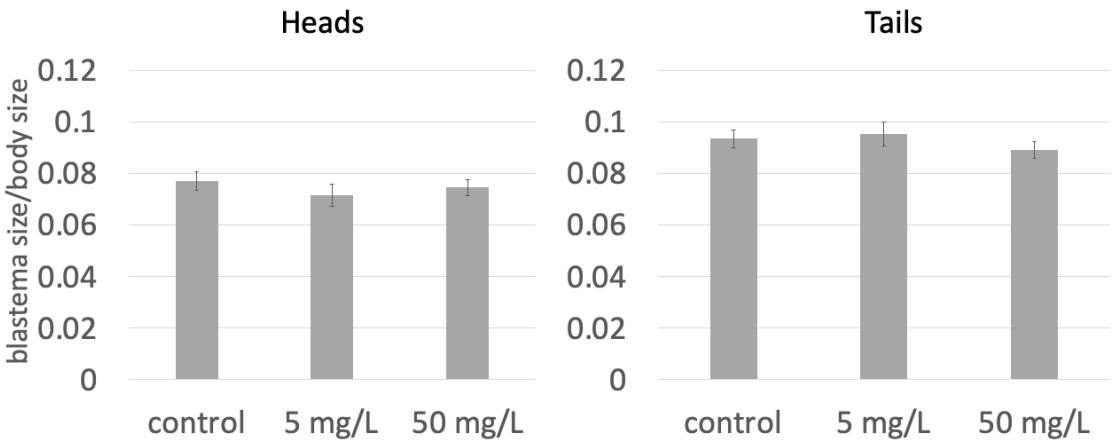

747

748 **Fig. B.7: Regenerative success described by blastema regeneration after TiO_2-NPs**
749 **exposure**. Blastema sizes of heads and tails exposed to 5 and 50 mg/L TiO_2-NPs, at 7 dpa,
750 corrected by the body size. Average relative blastema sizes in heads were: control = 0.077, 5
751 mg/L TiO_2 = 0.073, 50 mg/L TiO_2 = 0.075 and in tails were: control = 0.094, 5 mg/L TiO_2=
752 0.096 and 50 mg/L TiO_2 = 0.089. Results of three independent experiments, with in total ≥ 18
753 replicates per condition.

754

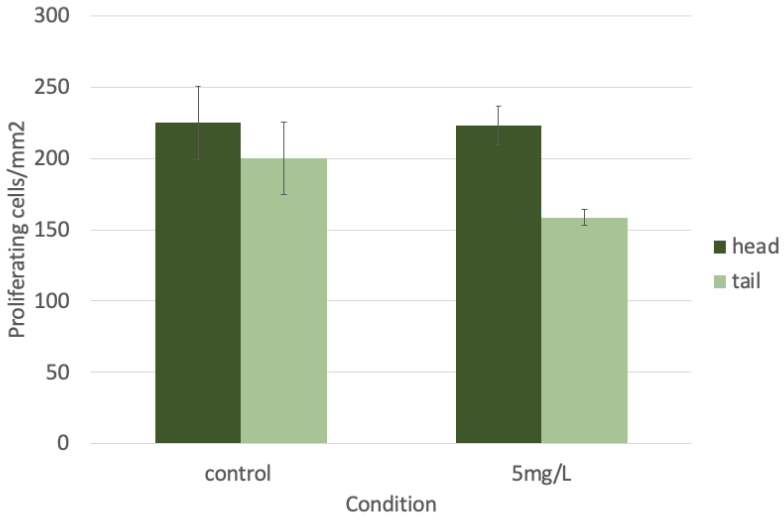

755

756 **Fig B.8: Stem cell proliferation after 14 days of exposure to TiO_2-NPs.** The number of
757 proliferating stem cells of heads and tails exposed to 5 mg/L TiO_2-NPs, at 14 dpa. Results of
758 one experiment with a total of at least seven replicates per condition.

759

Funding information

This work was supported by the Research Foundation Flanders (FWO) (G.0B83.17N, and N1522719), and the Bijzonder OnderzoeksFonds of Hasselt University (BOF20DOC14).

CRediT authorship contribution statement

Nathalie Leynen: Conceptualization, Methodology, Formal analysis, Visualization, Investigation, Validation, Writing – original draft. **Julie Tytgat**: Conceptualization, Formal analysis, Visualization, Investigation, Validation, Writing – original draft, Writing – review & editing. **Karolien Bijnens**: Conceptualization, Writing – review & editing **Vincent Jaenen**: Investigation, Writing – review & editing. **Tom Artois**: Resources, Funding acquisition.**Frank Van Belleghem**: Investigation, Methodology, Writing – review & editing. **Nelly Saenen**: Supervision, Writing – review & editing. **Karen Smeets**: Conceptualization, Supervision, Resources, Funding acquisition, Writing – original draft, Writing – review & editing.

Declaration of Competing Interest

(see template)

Acknowledgements

The authors thank Dr. Jan Mast and Dr. Eveline Verleysen from Sciensano for their expertise and help with the particle characterization. They thank Natascha Steffanie and Ria Vanderspikken for their skillful technical assistance.

References

Abbasi, R., et al. (2023). "Structural parameters of nanoparticles affecting their toxicity for biomedical applications: a review." J Nanopart Res **25**(3): 43. 10.1007/s11051-023-05690-w

Akanksha, G., et al. (2019). Challenges for Assessing Toxicity of Nanomaterials. Biochemical Toxicology. I. Muharrem, I. Olcay Kaplan and O. Gabrijel. Rijeka, IntechOpen**:** Ch. 4.

Boutillier, S., et al. (2020). "Food additives and the future of health: An analysis of the ongoing controversy on titanium dioxide." Futures **122**. 10.1016/j.futures.2020.102598

Cebrià, F. and P. A. Newmark (2007). "Morphogenesis defects are associated with abnormal nervous system regeneration following roboA RNAi in planarians."

Cesarini, G., et al. (2023). "Nanoplastic exposure inhibits feeding and delays regeneration in a freshwater planarian." Environmental Pollution **332**: 121959. https://doi.org/10.1016/j.envpol.2023.121959

Cruz-Rosa, S. and O. Pérez-Reyes (2023). "Titanium Oxide Nanoparticles as Emerging Aquatic Pollutants: An Evaluation of the Nanotoxicity in the Freshwater Shrimp Larvae Atya lanipes." Ecologies **4**(1): 141-151.

da Cunha, R. L. D. and L. de Brito-Gitirana (2020). "Effects of titanium dioxide nanoparticles on the intestine, liver, and kidney of Danio rerio." Ecotoxicology and Environmental Safety **203**. 10.1016/j.ecoenv.2020.111032

Dube, E. and G. E. Okuthe (2023). "Engineered nanoparticles in aquatic systems: Toxicity and mechanism of toxicity in fish." Emerging Contaminants **9**(2). 10.1016/j.emcon.2023.100212

EFSA (2021). "Titanium dioxide: E171 no longer considered safe when used as a food additive." from https://www.efsa.europa.eu/en/news/titanium-dioxide-e171-no-longer-considered-safe-when-used-food-additive. .

European Commission (2022). "ELEX:32022R0063: Commission Regulation (EU) 2022/63 of 14 January 2022 amending Annexes II and III to Regulation (EC) No 1333/2008 of the European Parliament and of the Council as regards the food additive titanium dioxide (E 171) (Text with EEA relevance).".

Gao, T., et al. (2022). "Exposure to polystyrene microplastics reduces regeneration and growth in planarians." Journal of Hazardous Materials **432**: 128673. https://doi.org/10.1016/j.jhazmat.2022.128673

Gottschalk, F., et al. (2009). "Modeled Environmental Concentrations of Engineered Nanomaterials (TiO2, ZnO, Ag, CNT, Fullerenes) for Different Regions." Environmental science & technology **43**(24): 9216-9222. 10.1021/es9015553

Gu, J., et al. (2021). "Titanium dioxide nanoparticle affects motor behavior, neurodevelopment and axonal growth in zebrafish (Danio rerio) larvae." Science of the Total Environment **754**. 10.1016/j.scitotenv.2020.142315

Hagstrom, D., et al. (2015). "Freshwater Planarians as an Alternative Animal Model for Neurotoxicology." Toxicological Sciences **147**(1): 270-285. 10.1093/toxsci/kfv129

Hong, F., et al. (2018). "Maternal exposure to nano titanium dioxide induces neurotoxic effects in offspring mice." J Biomed Sci **7**(2): 7.

Hu, C. C., et al. (2018). "Uptake of TiO2 Nanoparticles into C. elegans Neurons Negatively Affects Axonal Growth and Worm Locomotion Behavior." Acs Applied Materials & Interfaces **10**(10): 8485-8495. 10.1021/acsami.7b18818

Huang, X. Z., et al. (2018). "Oxidative stress induced by titanium dioxide nanoparticles increases under seawater acidification in the thick shell mussel Mytilus coruscus." Marine Environmental Research **137**: 49-59. 10.1016/J.marenvres.2018.02.029

Inoue, T., et al. (2004). "Morphological and functional recovery of the planarian photosensing system during head regeneration." Zoological Science **21**(3): 275-283. 10.2108/zsj.21.275

Ishitani, Y., et al. (2023). "Fascinating strategies of marine benthic organisms to cope with emerging pollutant: Titanium dioxide nanoparticles." Environmental Pollution **330**: 121538. https://doi.org/10.1016/j.envpol.2023.121538

ISO (2021). "ISO 18115-2:2021(en) Surface chemical analysis — Vocabulary — Part 2: Terms used in scanning-probe microscopy."

Joudeh, N. and D. Linke (2022). "Nanoparticle classification, physicochemical properties, characterization, and applications: a comprehensive review for biologists." Journal of Nanobiotechnology **20**(1): 262. 10.1186/s12951-022-01477-8

Jovanović, B., et al. (2016). "In situ effects of titanium dioxide nanoparticles on community structure of freshwater benthic macroinvertebrates." Environmental Pollution **213**: 278-282.

King, R. S. and P. A. Newmark (2013). "In situ hybridization protocol for enhanced detection of gene expression in the planarian Schmidtea mediterranea." Bmc Developmental Biology **13**. 10.1186/1471-213x-13-8

Kuper, C. F., et al. (2015). "Toxicity assessment of aggregated/agglomerated cerium oxide nanoparticles in an in vitro 3D airway model: The influence of mucociliary clearance." Toxicology in Vitro **29**(2): 389-397. 10.1016/j.tiv.2014.10.017

Lee, B., et al. (2019). "Silver nanoparticles induce reactive oxygen species-mediated cell cycle delay and synergistic cytotoxicity with 3-bromopyruvate in Candida albicans, but not in Saccharomyces cerevisiae." International Journal of Nanomedicine **14**: 4801-4816. 10.2147/ijn.S205736

Leynen, N., et al. (2019). "In vivo Toxicity Assessment of Silver Nanoparticles in Homeostatic versus Regenerating Planarians." Nanotoxicology **13**(4): 476-491. 10.1080/17435390.2018.1553252

Li, X. B., et al. (2019). "Prebiotic protects against anatase titanium dioxide nanoparticles-induced microbiota-mediated colonic barrier defects." Nanoimpact **14**. 10.1016/j.impact.2019.100164

Lowe, J. R., et al. (2015). "Ethanol exposure induces a delay in the reacquisition of function during head regeneration in Schmidtea mediterranea." Neurotoxicology and Teratology **48**: 28-32. 10.1016/j.ntt.2015.01.003

Luderwald, S., et al. (2019). "Exposure pathway dependent effects of titanium dioxide and silver nanoparticles on the benthic amphipod Gammarus fossarum." Aquatic Toxicology **212**: 47-53. 10.1016/j.aquatox.2019.04.016

Mendoza-Villa, F., et al. (2023). "Ecotoxicological Properties of Titanium Dioxide Nanomorphologies in Daphnia magna." Nanomaterials (Basel) **13**(5). 10.3390/nano13050927

Nanodefine (2016). "Development of an integrated approach based on validated and standardized methods to support the implementation of the EC recommendation for a definition of nanomaterial." FP7-NMP-2013-LARGE-7: NMP201314-3.

OECD (2016). "Titanium dioxide: summary of the dossier." Health and safety publications **ENV/JM/MONO(2016)25**.

Oliveira, M. S. S., et al. (2018). "Physiological evaluation of the behavior and epidermis of freshwater planarians (Girardia tigrina and Girardia sp.) exposed to stressors." Biology Open **7**(6). 10.1242/bio.029595

Parker, N. and A. A. Keller (2019). "Variation in regional risk of engineered nanoparticles: nanoTiO(2) as a case study." Environmental Science-Nano **6**(2): 444-455. 10.1039/c8en01079j

Pirotte, N., et al. (2015). "Reactive Oxygen Species in Planarian Regeneration: An Upstream Necessity for Correct Patterning and Brain Formation." Oxidative Medicine and Cellular Longevity **2015**. 10.1155/2015/392476

Ramsden, C. S., et al. (2009). "Dietary exposure to titanium dioxide nanoparticles in rainbow trout, (Oncorhynchus mykiss): no effect on growth, but subtle biochemical disturbances in the brain." Ecotoxicology **18**(7): 939-951. 10.1007/s10646-009-0357-7

Roberts-Galbraith, R. H., et al. (2016). "A functional genomics screen in planarians reveals regulators of whole-brain regeneration." Elife **5**. 10.7554/eLife.17002

Ross, K. G., et al. (2017). "Nervous system development and regeneration in freshwater planarians." Wiley Interdisciplinary Reviews-Developmental Biology **6**(3). 10.1002/wdev.266

Scimone, M. L., et al. (2014). "Neoblast Specialization in Regeneration of the Planarian Schmidtea mediterranea." Stem Cell Reports **3**(2): 339-352. 10.1016/j.stemcr.2014.06.001

Sheng, L., et al. (2016). "Mechanism of TiO2 nanoparticle-induced neurotoxicity in zebrafish (Danio rerio)." Environmental Toxicology **31**(2): 163-175. 10.1002/tox.22031

Tanvir, S., et al. (2015). "Toxicity Associated with the Photo Catalytic and Photo Stable Forms of Titanium Dioxide Nanoparticles Used in Sunscreen." MOJ Toxicology **1**: 00011. 10.15406/mojt.2015.01.00011

Torres-Garcia, D., et al. (2020). "Lethal and sub-lethal effects of nanosized titanium dioxide particles on Hydropsyche exocellata Dufour, 1841." Aquatic Insects **41**(1): 85-103. 10.1080/01650424.2020.1712422

Verleysen, E., et al. (2019). "Evaluation of a TEM based Approach for Size Measurement of Particulate (Nano)materials." Materials **12**(14). 10.3390/ma12142274

Wu, J. P. and M. H. Li (2018). "The use of freshwater planarians in environmental toxicology studies: Advantages and potential." Ecotoxicology and Environmental Safety **161**: 45-56. 10.1016/j.ecoenv.2018.05.057

Wu, Y. A., et al. (2010). "Effects of silver nanoparticles on the development and histopathology biomarkers of Japanese medaka (Oryzias latipes) using the partial-life test." Aquatic Toxicology **100**(2): 160-167. 10.1016/j.aquatox.2009.11.014

947 Zheng, Y. F. and B. Nowack (2021). "Size-Specific, Dynamic, Probabilistic Material Flow
948 Analysis of Titanium Dioxide Releases into the Environment." Environmental science &
949 technology **55**(4): 2392-2402. 10.1021/acs.est.0c07446
950
951